Research Article

Degradation of amaranth by persulfate activated with zero-valent iron: influencing factors, response surface modeling

Changye Yu[1] · Xian Lu[1] · Jinyu Lu[1] · Yinjiang Zhang[1]

Received: 24 January 2022 / Accepted: 23 June 2022
Published online: 12 December 2022

Abstract
In this study, zero-valent iron (ZVI) is applied to activate persulfate (PDS) for the degradation of amaranth (AMR). The effects of PDS concentration, ZVI concentration, solution pH , temperature, and reaction time on the degradation of AMR by the ZVI/PDS advance oxidation process are investigated. Sulfate and hydroxyl radicals are involved in the main reaction pathway of AMR and sulfate radical acts as a dominant oxidant. The CCD (central composite design) plan is chosen to build the RSM model for the prediction of AMR degradation. ANOVA analysis shows that the secondary fitting model had great fitness with $R^2 = 0.997$, $R^2_{adj} = 0.936$, p-value of lack of fit = 0.107. Optimum conditions for 98% AMR removal given by RSM are PDS concentration = 7.33 mM, ZVI dosage = 17.79 mM, initial pH 4.62, temperature = 59.49 °C, reaction time = 9.88 min which is proved to be very closed to the real removal rate of 96.78%. Sensitivity analysis indicates that the relative importance of the influencing parameters is of the following order: temperature, PDS concentration, pH , ZVI dosage, and reaction time. The PDS/ZVI system shows an acceptable RSE of about 75% and TOC removal of 85% on AMR oxidation. Finally, the possible pathway of AMR degradation is proposed.

Article Highlights

- High AMR degradation by PS through ZVI activation was achieved.
- The contributions of hydroxyl radicals and sulfate radicals were calculated.
- CCD of RSM was used to optimize the parameters in the AMR removal process.
- RSE and TOC were estimated to prove the efficiency of the PS/ZVI system.

Keywords Persulfate · Zero-valent iron · Response surface modeling · Amaranth

1 Introduction

Amaranth (AMR) is an alkaline azo dye that has a wide range of applications in natural and synthetic textiles, leather, paper, and resins [1, 2]. Because of its unappealing look and severe risk to human health, dye chemical contamination of water bodies frequently raises public consciousness and raises health concerns [3]. Azo dyes with the R–N–N–R functional group are of special concern because they can cause allergic and respiratory problems and tumors in animals [2, 4]. As a result, a substantial study has gone into finding effective strategies to remove azo dyes from wastewater.

Persulfate is set to become an arising aqueous oxidant among advanced oxidation processes (AOPs) for higher redox potential ($E_0 = 2.01$ V) than H_2O_2 ($E_0 = 1.76$ V) [5,

✉ Yinjiang Zhang, yjzhang@shou.edu.cn | [1]Engineering Research Center for Water Environment Ecology in Shanghai, College of Marine Ecology and Environment, Shanghai Ocean University, Shanghai 201306, China.

6]. Besides, it enjoys various benefits: a high solubility in water, non-specifically reactive, generally stable at room temperature, and widespread reactivity with environmental impurities [7]. Moreover, PDS showed high reaction stoichiometric efficiency (%RSE) which is the number of moles of probe degraded over the number of moles of PDS consumed [8]. Persulfate anions can turn into sulfate free radicals due to activation by a pH ysical method such as heat, ultrasound, ultraviolet, or by chemicals such as iron-based materials, biochar, or glucose (Eq. 1) [9–12]. Additionally, novel materials MOFs such as Co_3O_4/CNTs and MIL-88A were applied as a magnetic catalyst for persulfate activation [13, 14].

In recent years, iron-based metals were effective in activating persulfate. Ferrous ion (Fe^{2+}) has been reported to react successfully with PDS at a low ratio of [Fe^{2+}]/[PDS] to produce $SO_4^{\cdot-}$ (Eq. 2), which has been adopted for the elimination of refractory pollutants and pH armaceutical active ingredients in wastewater treatment [15]. However, sulfate radicals also react faster with ferrous ions than the formation of itself which leads to the loss of radicals and brings great limitations for practical use (Eq. 3) [16]. ZVI was proved to be a good source of Fe^{2+} for the activation of persulfate as an electron donor under both aerobic and anaerobic conditions (Eqs. 4–6) [17]. Besides, compared with dissolved Fe^{2+} persulfate is activated more successfully by ZVI because it can slowly release Fe^{2+}, which avoids $SO_4^{\cdot-}$ being scavenged by excess Fe^{2+} (Eq. 6) [18]. The generation of ferrous iron and recycling of ferric iron at the ZVI surface (Eq. 7) can avoid the accumulation of excess ferrous iron and reduce precipitation and sludge formation [19].

$$S_2O_8^{2-} \rightarrow 2SO_4^{-} \quad (1)$$

$$2Fe^{2+} + S_2O_8^{2-} \rightarrow 2SO_4^{-} \quad (2)$$

$$SO_4^{\cdot} + Fe^{2+} \rightarrow SO_4^{2-} + Fe^{3+} \quad (3)$$

$$2Fe + O_2 + 2H_2O \rightarrow 2Fe^{2+} + 4OH^{-} \quad (4)$$

$$Fe + 2H_2O \rightarrow 2Fe^{2+} + 2OH + H_2 \quad (5)$$

$$2Fe + 2H^{+} \rightarrow Fe^{2+} + H_2 \quad (6)$$

$$Fe + 2Fe^{3+} \rightarrow 3Fe^{2+} \quad (7)$$

RSM is a statistical-based design method that can assess the individual and interaction impacts of independent variables on complex systems and improves response conditions through a limited number of experiments [20]. Central composite design (CCD) has been proved useful for building the prediction model and optimizing the parameters to achieve the effective degradation of target pollutants [21–23].

In the next section, we explain the procedure and the basic theory of the following experiments. Sections 3.1–3.7 shows the effects of PDS concentration, ZVI dosage, solution pH , temperature, and anions on the AMR degradation process and the dominant radical of the degradation process. In Sect. 3.7, we present the RSM model of the AMR oxidation process and optimize the parameters to reach a high degradation rate. Moreover, in Sects. 3.8–3.9 we figure out the estimation of reaction stoichiometric efficiency (RSE) and the removal of total organic carbon (TOC). In the last section, a possible pathway for AMR degradation is proposed through HPLC–MS analysis.

2 Materials and methods

2.1 Chemicals

Ultra-pure water is produced by a Millipore milli-Q system for all solutions preparation. All chemicals used in this study were reagent grade and were used as received without further purification. Sodium-persulfate ($Na_2S_2O_8$, 98%), amaranth ($C_{20}H_{11}N_2Na_3O_{10}S_3$) (99.5%), Zero-valent iron (Fe^0, 99%, 0.15 mm), Tert-butanol (TBA, 99.7%), Methanol (MeOH, 99.8%), Sodium chloride (NaCl, 99.8%), Sodium bicarbonate ($NaHCO_3$, 99%) were purchased from Aladdin and Sino-pH arm.

2.2 Experiments procedures

Batch degradation experiments were carried out to investigate the effects of several parameters (PDS concentration, ZVI dosage, solution pH , temperature, reaction time, and anions) on persulfate-ZVI oxidation. Each batch test was performed in a 500 mL cylindrical amber glass bottle placed in a rotary shaker at 100 rpm. Stock solutions of AMR (50 mg/L) were prepared in deionized water for each batch experiment and well-kept ZVI powder was then added to the solution. The initial pH of each solution was adjusted with 1 M sodium hydroxide (NaOH) or sulfuric acid (H_2SO_4) and examined by a digital pH meter. PDS concentration was varied from 1 to 8 mM, ZVI concentration ranged from 1 to 30 mM, pH varied from 3 to 11, selected anions like bicarbonate and chloride ion varied from 1 to 30 mM, and the temperature was maintained at 25 °C, 30 °C, 40 °C, 50 °C, and 60 °C for each run. PDS was added to the solutions containing AMR and ZVI to initiate the reaction. At regular time intervals, the 3 mL sample aliquots were withdrawn with syringes and filtered using

0.22 µm polytetrafluoroethylene syringe filters (Millipore, German). All samples were taken into 5 mL vials containing 0.2 mL of 0.1 mol/L methanol to quench the reaction. Quenching reactions were performed to figure out the dominant radical species responsible for AMR degradation. Methanol (MeOH) and Tert-Butyl alcohol (TBA) were chosen to be the radical scavengers where MeOH is a radical scavenger for both ·OH and $SO_4^{\cdot-}$ while TBA is only for ·OH. All experiments were conducted in triplicate, and the results were shown as means to ensure reproducibility.

2.3 Design of experiment and RSM

Response surface methodology (RSM) was chosen to optimize AMR removal efficiency using five independent factors based on the previous single parameters results: PDS concentration, ZVI concentration, solution pH , temperature, and reaction time. RSM experiment was designed through the central composite design (CCD). The coded and actual levels of parameters used for RSM are given in Table 1. The experiments were conducted according to the runs according to Table 2.

Experiment results were plotted into a second-order polynomial equation (Eq. 8) to correlate the response to independent parameters.

$$Y_{AMR} = z_0 + \sum_{j=1}^{k} z_j x_j + \sum_{j=1}^{k} z_{jj} x_j^2 + \sum_{i=1}^{k} \sum_{j=1}^{k} z_{jj} x_i x_j \quad (8)$$

where Y_{AMR} is the response (%), X_j stands for the parameters Z_0, Z_i, Z_{jj}, and Z_{ij} are the regression constants. The reliability of the model equation was evaluated by a statistical tool, analysis of variance (ANOVA) which compares variation by calculating residuals of the variance using the mean *F*-test [24, 25].

2.4 Analysis method

Persulfate anion concentration was measured by iodometric titration with sodium thiosulfate using a UV–VIS spectropH otometer according to the detection method developed by Liang et al. [26]. PDS concentration calibration curves were performed within a range of 0.1–10 mM.

TOC measurements were conducted using a TOC-L series analyzer by Shimadzu. The system measures the different conductivity of the CO_2 percolating specific membrane to determine the amount of CO_2 produced by the AMR oxidation.

The intermediates were identified by the high-performance liquid chromatograpH y-mass spectrometry (HPLC–MS, Shimadzu LCMS 8050). The reversed-pH ase C18 column (250 mm × 4.6 mm) was used with the column temperature maintained at 40 °C. The acetonitrile–water (90:10, v/v) was chosen as the mobile pH ase with a flow rate of 0.30 mL/min and a retention time of 30 min.

The residual concentration of AMR was measured by a UV–visible spectrometer at the peak wavelength of 520 nm. The contribution of the two radicals to AMR degradation was calculated by the degradation speed rate of each run. Degradation of AMR in ZVI/PDS processes was typically described as a pseudo-first-order reaction (Eq. 9):

$$\mathrm{Ln}\left(\frac{[\mathrm{AMR}]_t}{[\mathrm{AMR}]_0}\right) = -k_{obs} \times t \quad (9)$$

where [AMR] and $[AMR]_0$ (mg/L) stand for the concentration of AMR at time *t* and 0, respectively; *t* (min) represents reaction time; k_{obs} (min^{-1}) represents the reaction rate constant in ZVI/PDS systems.

The suitability of the prediction model equation for AMR was evaluated using the statistical tool ANOVA utilizing the Design Expert 11. The numerical optimization module in the same software was also applied to obtain the optimal parameter values under a certain removal rate.

3 Results and discussion

3.1 Effect of PDS on the degradation of AMR

It has been found that the initial concentration of PDS will directly change the concentration of active free radicals generated to affect the degradation rate of AMR. To

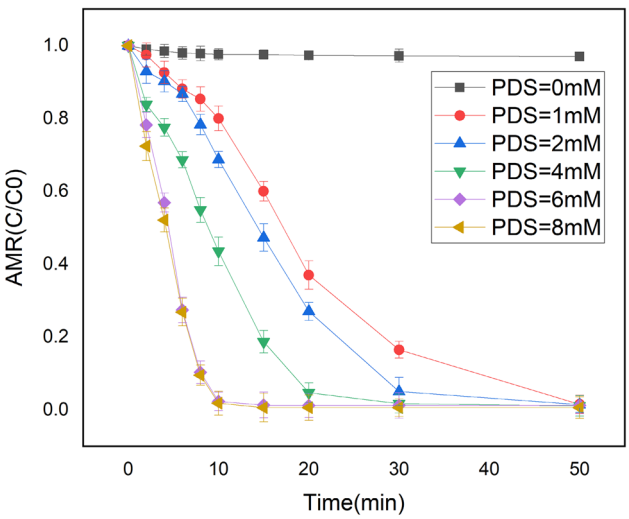

Fig. 1 Effect of PDS concentration on AMR degradation in persulfate–ZVI system. Change of the persulfate concentration over time $[AMR]_0$ = 50 mg/L, $[PDS]_0$ = 1-8 mM, $[ZVI]_0$ = 5 mM, Temp. = 25 °C, pH 7.0

explore the effect of PDS on the degradation, a set of PDS concentrations (1, 2, 4, 6, 8 mM) was applied while other parameters were kept constant. Results in Fig. 1 indicated that the AMR removal rate increased with an increasing initial concentration of PDS due to more persulfate radicals. At a higher initial PDS concentration, more PDS molecules would react with Fe^0 and Fe^{2+}, resulting in more $SO_4^{\cdot-}$ and ·OH radicals [27]. When the concentration of sodium persulfate is 6 mM, the degradation efficiency reached 98.2% at 50 min. However, no enhanced removal was observed when the concentration of PDS increased from 6 to 8 mM. These results were similar to a previous study using PDS for the decolorization of carbamazepine [28]. This pH enomenon could be explained by the reduction of sulfate radical and unproductive decomposition of $S_2O_8^{2-}$ (Eqs. 10, 11) [29, 30]. This implied that a much higher concentration of sodium persulfate could not significantly improve the degradation efficiency, so the most suitable concentration of sodium persulfate in this study is 6 mM.

$$SO_4^{\cdot-} + S_2O_8^{2-} \rightarrow SO_4^{2-} + S_2O_8^{\cdot-} \quad (10)$$

$$S_2O_8^{2-} + HO^{\cdot} \rightarrow S_2O_8^{\cdot-} + OH^- \quad (11)$$

3.2 Effect of ZVI dosage on the degradation of AMR

The effect of initial ZVI concentration (range from 1 to 30 mM) on AMR removal in the ZVI/PDS system was investigated while maintaining AMR at 50 mg/L, persulfate concentration at 6 mM, the temperature at 25 °C, and initial pH value of 7.0. Figure 2 shows as the ZVI concentration ranged from 1 to 30 mM, more AMR moles were eliminated at the same reaction time. The results showed that the degradation of AMR by PDS was significantly dependent on ZVI concentration, and the removal rate can reached 99% at 20 min in a high ZVI dosage (15 mM). This study indicated that ZVI had a positive impact on the degradation efficiency of AMR in the ZVI/PDS system due to the release of Fe^{2+} from ZVI. During the oxidation process by persulfate, more dissolved Fe^{2+} was supplied to the system with a higher ZVI concentration, which can activate persulfate to sulfate radicals and enhance AMR removal efficiency [31]. The degradation rate of AMR is very fast at first, but the degradation rate becomes slower as the oxidation progresses gradually. These results were similar to a previous study using ZVI/PDS system for oxidation of bentazon [17].

3.3 Effect of pH on the degradation of AMR

Previous studies have shown that pH can play an important role in iron-catalyzed reactions, and acidic conditions are conducive to ZVI-activated persulfate oxidation [32]. Therefore, a set of pH values ranging from 3 to 11 was applied to the degradation of AMR by ZVI-persulfate. The results (Fig. 3) show that the degradation efficiency of AMR is significantly influenced by the solution pH . When solution pH was 3.0, the degradation rate of AMR is 88.23% at 10 min and reached almost 100% at 15 min. Respectively, at pH 9.0 and 11.0, the removal rates of AMR at 10 min were 40.59% and 24.52%. This is because

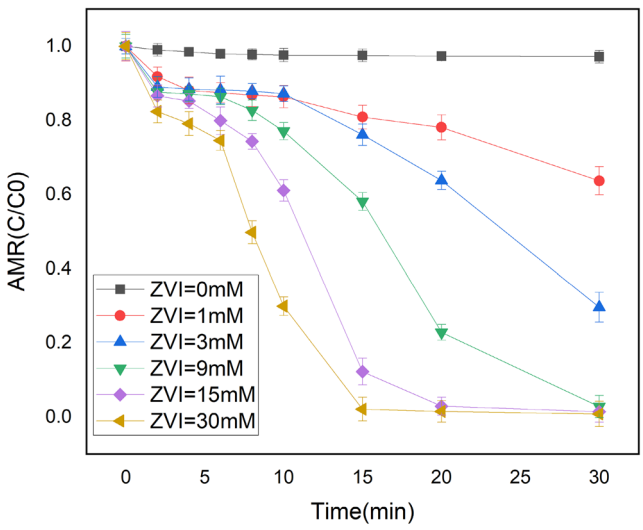

Fig. 2 Effect of ZVI concentration on AMR degradation in persulfate–ZVI system. $[AMR]_0 = 50$ mg/L, $[PDS]_0 = 6$ mM, $[ZVI]_0 = 1–30$ mM, Temp. = 25 °C, pH 7.0

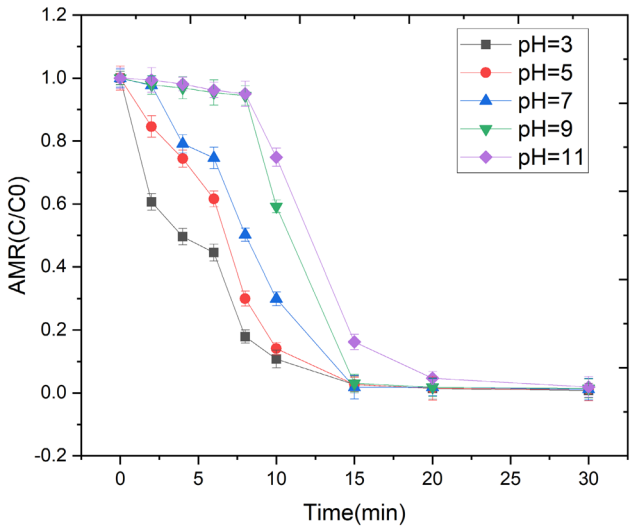

Fig. 3 Effect of solution pH on AMR degradation in persulfate–ZVI system. $[AMR]_0 = 50$ mg/L, $[PDS]_0 = 6$ mM, $[ZVI]_0 = 15$ mM, Temp. = 25 °C. pH i and pH f are summarized in Table 3

PDS can be activated directly or by Fe^{2+} to produce $SO_4^{\cdot-}$ under acidic conditions [33]. Table 3 showed that the pH of the solution decreased to an acidic value (2.8–5.5) whatever the initial pH was and then kept stable till the reaction finished. Similar pH changes were reported in the previous research [34, 35]. This was because of the deduction of the OH^- through the hydrolysis of Fe^{3+} and the conversion from $SO_4^{\cdot-}$ to ·OH under different pH conditions (Eqs. 12–14) [35, 36]. It could be inferred that ZVI/persulfate systems showed successful adaptability to a wide range of the initial pH .

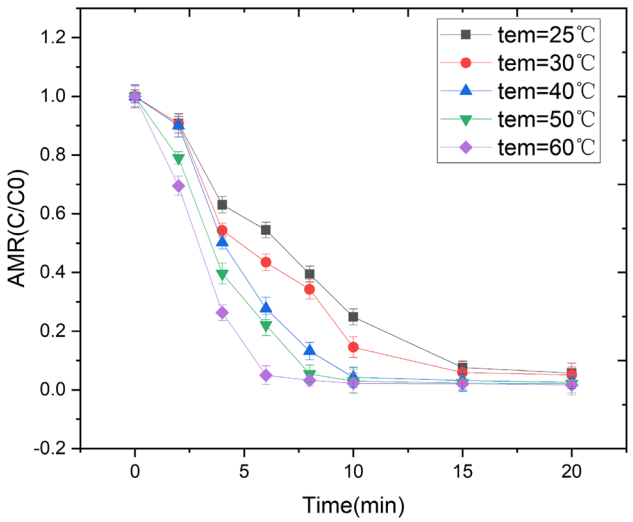

Fig. 4 Effect of temperature on AMR degradation in persulfate–ZVI system. $[AMR]_0 = 50$ mg/L, $[PDS]_0 = 6$ mM, $[ZVI]_0 = 15$ mM, Temp. = 25–60℃, pH 7.0

$$SO_4^{\cdot-} + H_2O \rightarrow SO_4^{2-} + {}^{\cdot}OH + H^+ \quad (12)$$

$$SO_4^{\cdot-} + {}^{\cdot}OH \rightarrow SO_4^{2-} + H^+ + 0.5O_2 \quad (13)$$

$$SO_4^{\cdot-} + OH^- \rightarrow SO_4^{2-} + {}^{\cdot}OH \quad (14)$$

3.4 Effect of temperature on the degradation of AMR

The effect of temperature on the degradation of AMR was studied under the conditions of 25 °C, 30 °C, 40 °C, 50 °C, and 60 °C. The result showed that temperature is an important parameter that determines the degree of PDS activation and degradation of AMR. As shown in Fig. 4, the removal rate at 8 min of AMR at 25 °C is 59.17%, while the degradation rate at 60 °C is 96.99%. As the reaction temperature increased from 25 to 60 °C, the time to reach removal rate of about 99% was reduced from 20 to 10 min. The result indicates that thermal energy can also activate persulfate to sulfate radicals. Under high-temperature conditions, more O–O bonds in the sodium persulfate molecules will be broken resulting in a large amount of $SO_4^{\cdot-}$. Increasing temperature improved iron oxidation as well resulting in a quicker release of Fe^{2+} in the medium. This result agreed with a previous study in which raising the reaction temperature from 20 to 60 °C leads to the full removal of trichloroethylene (TRI) by thermally activated PDS [37]. Although the high temperature was conducive to the degradation of AMR, it might not be a promising way in actual engineering because higher reaction temperature requires more operating cost. Therefore, this

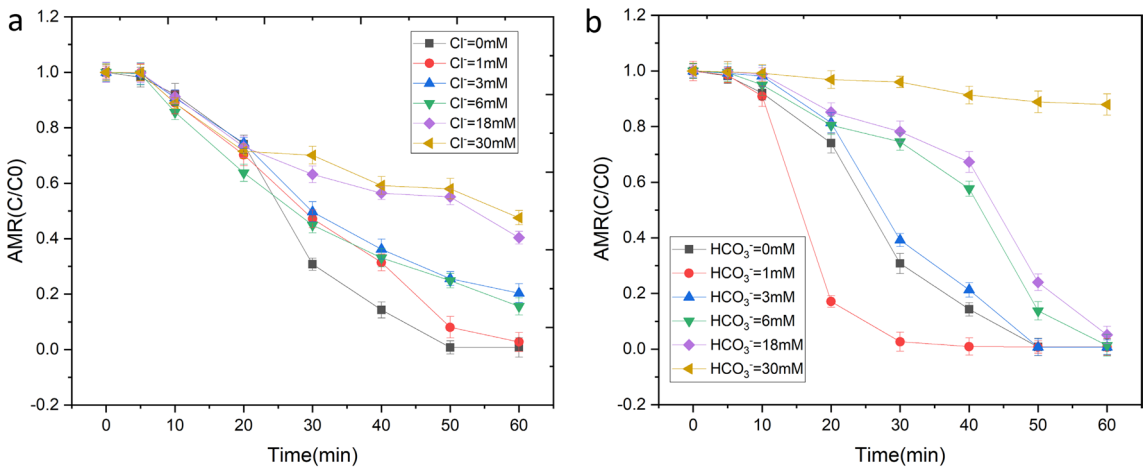

Fig. 5 **a** Effect of chloride ions on AMR degradation in persulfate–ZVI system. **b** Effect of bicarbonate on AMR degradation in persulfate–ZVI chloride ions system. $[AMR]_0 = 50$ mg/L, $[PDS]_0 = 6$ mM, $[ZVI]_0 = 15$ mM, Temp. = 25 °C, pH 7.0, $[Cl^-] = 1$–30 mM, $[HCO_3^-] = 1$–30 mM

experiment chose 40 °C as the most suitable reaction temperature.

3.5 Effect of anions on the degradation of AMR

Figure 5b showed that chloride ion generally had negative effects on AMR degradation within the concentration range from 1 to 30 mM. The reduction of AMR was suppressed by Cl^-, but the degree of the suppression on the reaction has no obvious positive or negative correlation with the concentration of chloride ions. Chloride ion can react with activation products $SO_4^{\cdot-}$ and ·OH to form chloride radicals, such as Cl· and $HOCl^{\cdot-}$ which possess lower redox potential (Eqs. 15–16). Studies have shown that the presence of Cl^- promotes the formation of short-term free radicals through free radical propagation reactions via chain reactions [38].

$$Cl^- + SO_4^{\cdot-} \rightarrow Cl^{\cdot} + SO_4^{2-} \quad (15)$$

$$Cl^- + {}^{\cdot}OH \rightarrow HOCl^{\cdot-} \quad (16)$$

Figure 5b shows that bicarbonate ion firstly promoted the degradation of AMR by ZVI-persulfate and then have negative effects as its concentration increased from 1 to 30 mM. The degradation of AMR was promoted when the HCO_3^- concentration was 1 mM. As the concentration increased from 3 to 30 mM, the negative effect continued to be strengthened. The degradation of AMR was almost inhibited when the concentration of HCO_3^- reached 30 mM. Studies have shown that HCO_3^- can quench part of $SO_4^{\cdot-}$/OH and produce less active $HCO_3^{\cdot}$ and $CO_3^{\cdot-}$ (Eqs. 17–18) [39]:

$$SO_4^{\cdot-} + HCO_3^- \rightarrow SO_4^{2-} + HCO_3^{\cdot} \quad (17)$$

$${}^{\cdot}OH + HCO_3^- \rightarrow CO_3^{\cdot-} + H_2O \quad (18)$$

3.6 Dominant radical verification and contribution

It was reported that MeOH reacts at a similar rate with $SO_4^{\cdot-}$ ($9.7\times108\ M^{-1}\ s^{-1}$) and ·OH ($1.1\times107\ M^{-1}\ s^{-1}$), which made it an efficient quencher for both $SO_4^{\cdot-}$ and ·OH [40]. TBA was chosen to quench ·OH because its rate constant with ·OH ($3.6\times108\ M^{-1}\ s^{-1}$) is 1000-times faster than that with $SO_4^{\cdot-}$ [41]. The free radical quenchers were added according to the molar ratio of 50:1 with PDS. Figure 6 shows the AMR removal by ZVI/PDS with and without scavenging agents. Radical-scavenging tests were conducted using TBA and EtOH, the oxidation reaction of AMR slowed down when TBA or MeOH existed, indicating

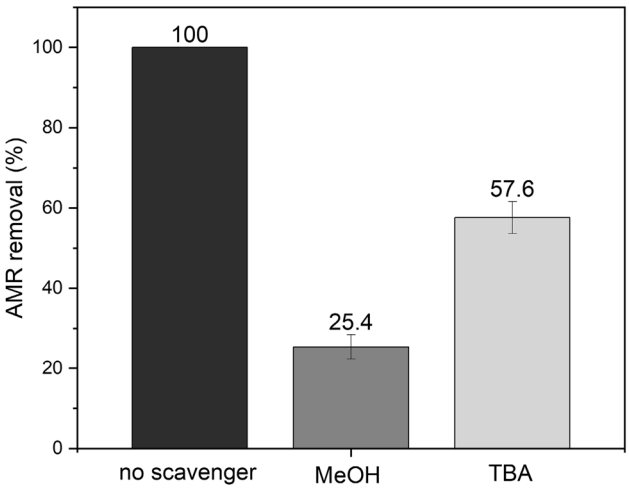

Fig. 6 Effect of quench scavenger on AMR degradation in persulfate–ZVI system. $[AMR]_0 = 50$ mg/L, $[PDS]_0 = 6$ mM, $[ZVI]_0 = 15$ mM, Temp. = 25 °C, pH 7.0, [MeOH] = 5 mM, [TBA] = 5 mM time = 20 min,

that $SO_4^{\cdot-}$ and ·OH played important roles in ZVI-persulfate oxidation. The presence of TBA reduced the AMR removal from 100% (reaction without scavengers) to 57.6% at 20 min and while MeOH is 25.4%, respectively. This decrease indicates that the contribution rate of $SO_4^{\cdot-}$ and ·OH was 42.4% and 29.2%. It can thus be concluded that the dominant free radical of the ZVI/PDS system is $SO_4^{\cdot-}$. The result was in agreement with previous AOP studies on persulfate [42, 43].

3.7 RSM statistical analysis

3.7.1 Model establishment and validation

The ANOVA analysis for the obtained quadratic model is shown in Table 4. Figure 7a displayed the closeness of the actual and predicted responses and the residuals distribution is shown in Fig. 7b. R^2 of Model equation was 0.9772 which indicated the reliability of the model in predicting AMR degradation; Eq. (19) was applied to the AMR degradation model:

$$\begin{aligned} Y = {} & 63.11 + 13.92A + 7.70B - 8.45C + 15.43D \\ & + 2.43E + 4.02AB - 3.59AC + 2.63AD \\ & + 3.19AE - 1.66BC + 1.31BD + 1.33BE \\ & + 0.38CD + 2.49CE - 2.12DE - 6.87A^2 \\ & - 22.88B^2 + 3.25C^2 + 3.62D^2 - 1.14E^2 \end{aligned} \quad (19)$$

where A = PDS concentration (mM), B = ZVI concentration (mM), C = pH , D = temperature (℃) and E = reaction time (min). The sensitivity analysis indicated that temperature is the most influential input process parameter followed

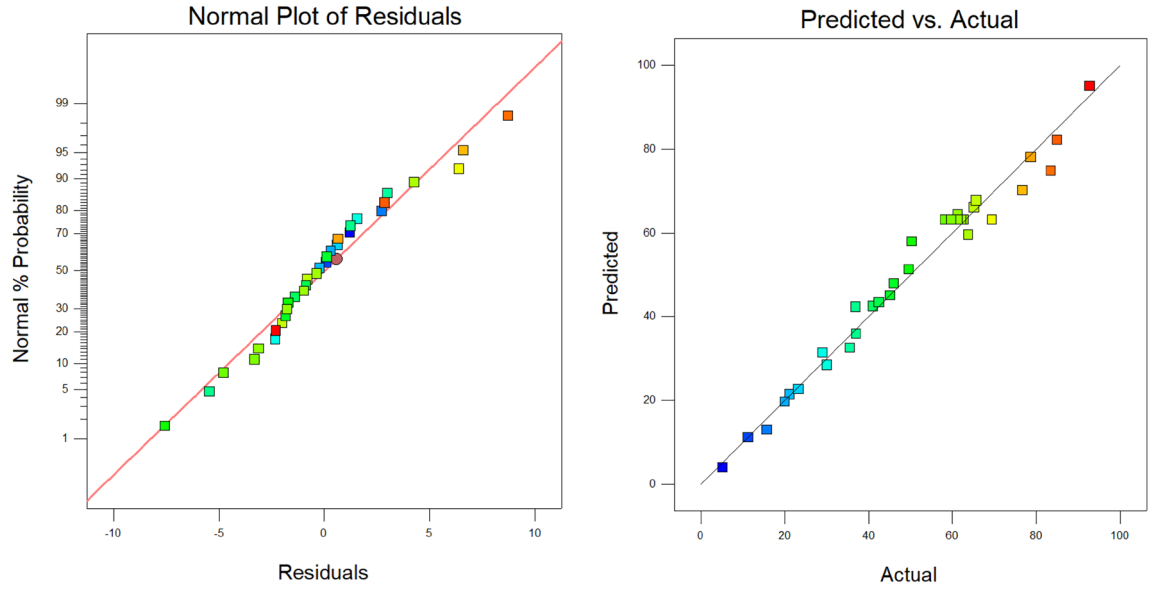

Fig. 7 **a** The normality plot of the residuals for the AMR reduction. **b** Scatter plot of predicted vs actual for the percent removal of AMR

by PDS concentration, pH , ZVI concentration, and reaction time. Since *A*, *B*, *C*, *D*, *AB*, *AC*, *AE*, B^2 are significant terms (*p*-value < 0.05) among the model factors, it implied that they have a greater impact on AMR removal. Thus, the model equation Eq. (19) was improved to be Eq. (20) for a more accurate prediction of the process:

$$Y = 63.11 + 13.92A + 7.70B - 8.45C + 15.43D + 4.02AB - 3.59AC + 3.19AE - 22.88B^2 \quad (20)$$

3.7.2 Statistical analysis

According to the results in Table 2, we can see that the most important interactions were AB, AC, and AE for their high significance, but the most relevant was AB according to the sum of squares term. Figure 8 showed the interactions between the different parameters which were significant (*p*-value < 0.05). The corresponding effects of two parameters were plotted into 2D contour (Fig. 9a–c) and 3D surface (Fig. 9d–f) which could help to identify the type of interactions between the selected variables. Combining the results in Fig. 9 and Table 5, the 2D or 3D surface plot shaped convex when a coefficient estimate of the factor is positive (AB and AE). In the contrast, the surface is concave which corresponds to the negative coefficient estimate (AC).

Coming to the interaction between AB, we can see that an increase in PDS concentration leads to an increase in AMR degradation as expected whatever the ZVI dosage. On the other hand, less significant interactions were observed on AC (PDS concentration and pH) and AE (PDS concentration and time). Considering AC, the removal rate decreased as the pH increased, because Fe^{2+} concentration will go down as the reaction with OH^- at alkaline pH which will inhibit the activation of PDS. 76.79% AMR reduction was accomplished at PDS = 8 mM, ZVI = 17.5, pH 7, temperature = 42.5 °C and reaction time = 10 min (Fig. 8a and b). When the removal rate was fixed to a higher target, more PDS concentration and a lower pH were required, which indicated that an acidic environment is more favorable for AMR degradation because ZVI tended to release more Fe^{2+} with a high H+ ion concentration (Fig. 8c and d). The data given in Fig. 8e and f depicted that increases in both PDS concentration and contact time result in a much higher removal of AMR. This may be as a result more $SO_4^{\bullet -}$ was produced which participated in the oxidation. The results showed great consistency with the previous single parameters experiment.

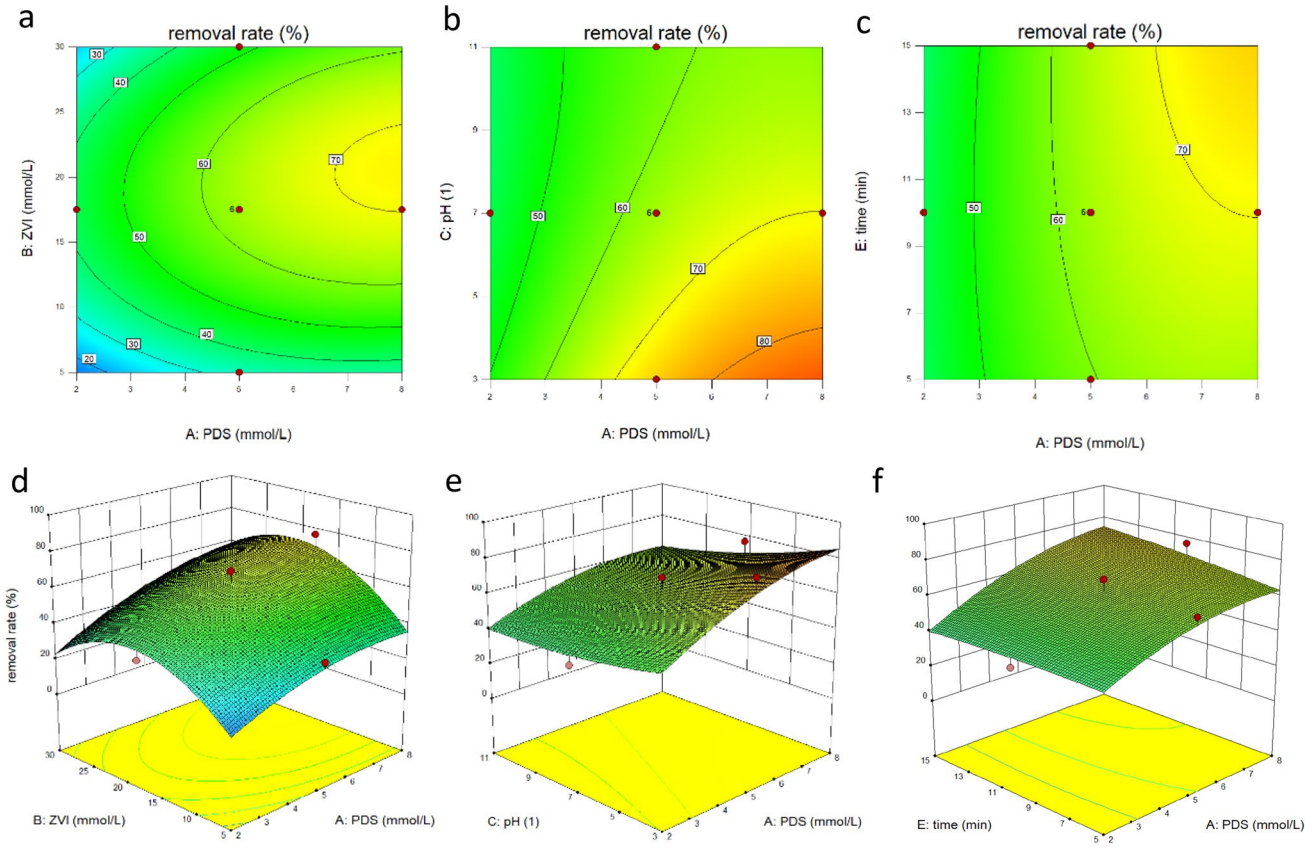

Fig. 8 2D contour and 3D plots of the interactions between different parameters: PDS and ZVI (**a**, **d**), PDS and pH (**b**, **e**), PDS and reaction time (**c**, **f**)

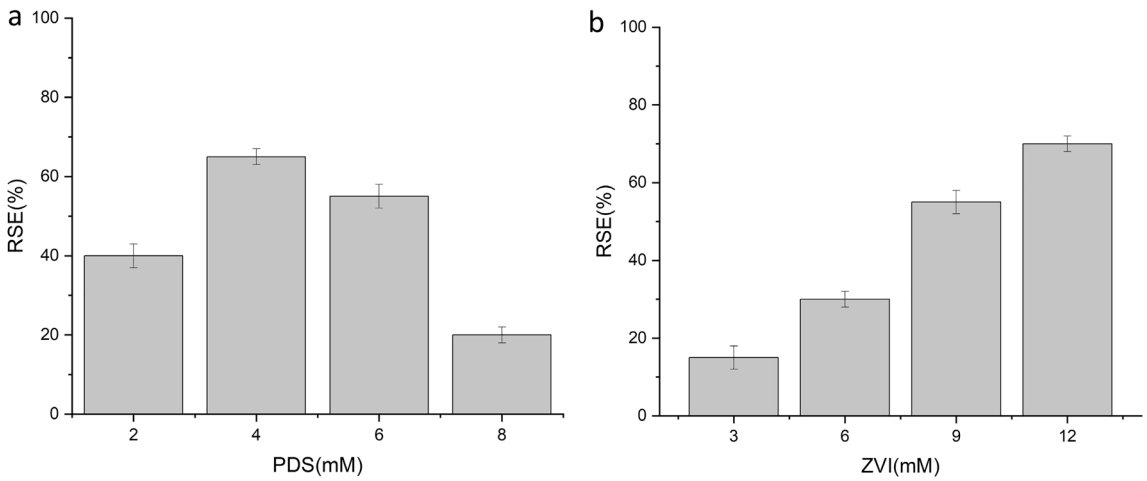

Fig. 9 **a** Reaction stoichiometric efficiency (RSE) calculated for the different PDS concentration. Experimental conditions: $[AMR]_0 = 50$ mg/L, $[ZVI]_0 = 10$ mM, Temp. = 25 °C, pH 7.0. **b** Reaction stoichiometric efficiency (RSE) calculated for the different PDS concentration. Experimental conditions: $[AMR]_0 = 50$ mg/L, $[PDS]_0 = 4$ mM, Temp. = 25 °C, pH 7.0

3.7.3 RSM optimization and validation of the model

The optimum conditions were obtained using the numerical optimization tool in Design Expert 11 by setting each parameter within the range and the target removal efficiency of 98% at 10 min. RSM gave optimized parameters combination (at PDS concentration = 7.33 mM, ZVI dosage = 17.79 mM, initial pH 4.62, temperature = 59.49℃, reaction time = 9.88 min) at desirability of 98%. The predictions were validated by triplicate repeating experiments at the optimum condition and the average removal efficiency was 96.67%. The results proved that the RSM quadratic model had the reliability to predict and optimize the degradation of AMR. This study is similar to that of Islahuddin and Halmi who obtained the turbidity (98.4%) for RSM optimization [44].

3.8 Estimation of reaction stoichiometric efficiency (RSE)

Reaction stoichiometric efficiency (RSE) is the effective PDS moles ratio calculated by the number of degraded AMRs moles versus the number of consumed PDS moles. Figure 9 summarizes the RSE values of AMR degradation under the condition of different ZVI dosages and PDS concentrations after 20 min. As can be noticed in Fig. 9a, the RSE values were inversely related to PDS concentration while there was a positive correlation between RSE values and ZVI dosage. When PDS concentration is 4 mM, the average RSE is close to 65%, respectively while it dropped to 19% when PDS was 8 mM. Figure 9b reveals the fact that high ZVI benefits an acceptable RSE of the PDS/ZVI system. This can be explained by the more effective activation of PDS molecules due to an increasing density of Fe^{2+} ions. RSE can reached the maximum of 78% under the condition at PDS = 4 mM, Z VI = 12 mM, pH 7, temperature = 25℃ and reaction time = 20 min. The maximum RSE above 75% showed clearly the advantage of PS/ZVI for AMR degradation.

3.9 Estimation of total organic carbon (TOC)

The TOC removal rate is widely used as a key parameter to measure the efficiency of pollutant degradation. The TOC of the AMR solution before and after the treatment was estimated and the results were shown in Fig. 10. The removal of TOC depended upon the initial PDS concentration and a higher PDS concentration could improve the removal of TOC. Despite the decent RSE with the increase of PDS concentration, the TOC of the AMR solution decreased rapidly under higher ZVI dosage and reached the acceptable level of about 80% in 20 min. According to the previous results of this study, PDS/ZVI system showed the ability to efficient removal for AMR and TOC from the solution.

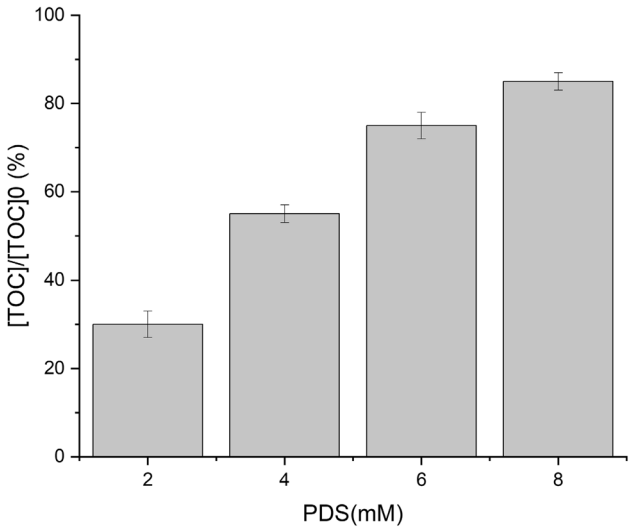

Fig. 10 TOC of AMR solution treated in ZVI/PDS system of different PDS concentrations. Experimental conditions: $[AMR]_0$ = 50 mg/L, $[TOC]_0$ = 28.8 mg/L, $[PDS]_0$ = 2–8 mM, $[ZVI]_0$ = 15 mM, Temp. = 25 °C, pH 7.0, reaction time = 20 min

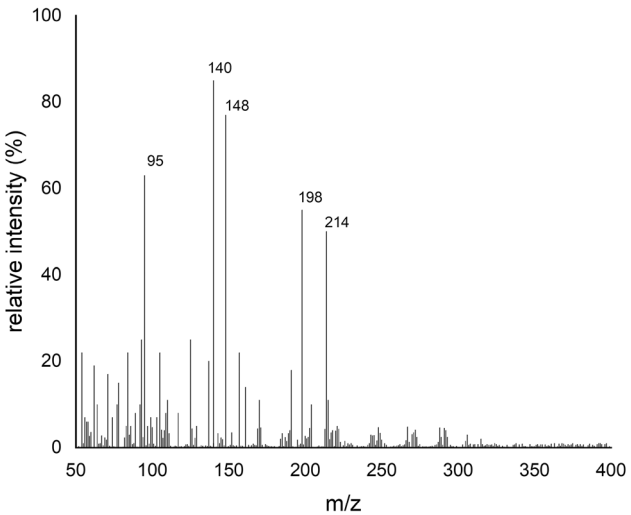

Fig. 11 HPLC–MS ESI total ion chromatograms of AMR solution treated in ZVI/PDS system with a retention time of about 3 min. Experimental conditions: $[AMR]_0$ = 50 mg/L, $[PDS]_0$ = 6 mM, $[ZVI]_0$ = 15 mM, Temp. = 25 °C, pH 7.0, reaction time = 5 min

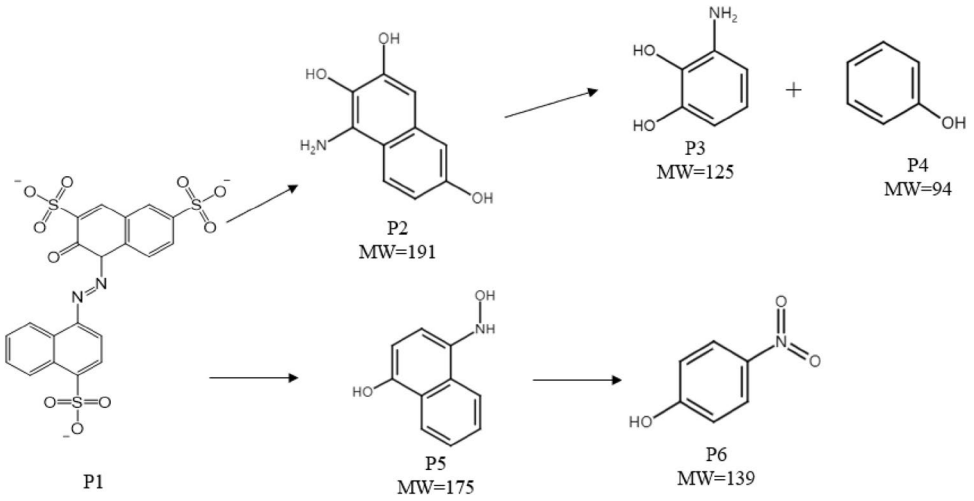

Fig. 12 A logical degradation pathway of AMR by PS/ZVI system

Table 1 Process variables and their actual and coded levels used for CCD

Factor	Name	Units	Min	Max	Coded	Values	Mean	Std. Dev
A	PDS	mmol/L	2	8	−1 = 2	1 = 8	5	2.286
B	Fe	mmol/L	5	30	−1 = 5	1 = 30	17.5	9.525
C	pH	1	3	11	−1 = 3	1 = 11	7	3.048
D	Tem	Celsius	25	60	1 = 25	1 = 60	42.5	13.335
E	time	min	5	15	−1 = 5	1 = 15	10	3.810

3.10 AMR degradation pathway

In the practical treatment of dye wastewater, it is important to figure out whether AMR was fully destructed by PDS/ZVI system. The AMR degradation pathway could be useful to evaluate its toxicity in the degradation process and analyze the mechanism of AMR degradation by the PDS/ZVI system. Samples from the reaction system were analyzed using HPLC–MS and the potential intermediates are summarized in Table S5 according to the mass spectrum results shown in Fig. 11. The material of retention time 5 min on HPLC showed m/z values of 95, 140, 148, 198, and 214. Based on these intermediates and relative studies [45–47], a logical degradation pathway was depicted in Fig. 12. At first, AMR was dissociated to become P1, the N–N bonds inside P1 were attacked and the sulfonate group of P1 might be substituted with the hydroxyl group to form P2 (MW = 191) and P5 (MW = 175) by the generated hydroxyl and persulfate radicals which causing the observed discoloration. Ring-opening reactions might occur in P2 to become P3 (MW = 125) and P4 (MW = 94). P5 might undergo ring-opening reactions or the NH-OH group was oxidated to the NO2 group to form P6 (MW = 139). The potential intermediates were further degraded to low molecular weight compounds such as short-chain carboxylic acids and would be finally mineralized into CO_2 and H_2O.

4 Conclusions

The findings of this work have successfully confirmed that the ZVI/persulfate system is an effective way to degrade AMR. In ZVI/persulfate system the decomposition of persulfate occurred more rapidly due to the release of Fe^{2+} from ZVI. The degradation rate of AMR was positively correlated with the increase in PDS concentration and ZVI dosage. High temperature and low pH could significantly promote the degradation of AMR. Both chloride ion and high concentration of bicarbonate ion suppressed the oxidation ability of the ZVI/PDS system while low concentration of bicarbonate ion resulted in enhanced AMR degradation. $SO_4^{\cdot-}$ and ·OH were confirmed as the key radicals, and $SO_4^{\cdot-}$ contributed more to the reaction. Parameters like PDS concentration, ZVI dosage, solution pH , temperature, and reaction time were considered statistically for optimization using the RSM technique during AMR elimination. The CCD model of RSM with $R^2 = 0.997$, $R^2_{adj} = 0.936$, p-value of lack of fit = 0.107 successfully fitted the degradation process of AMR. The optimal

Table 2 Full factorial CCD matrix and Experimental AMR removal efficiency

run	PDS(mM)	ZVI(mM)	pH	Temperature(℃)	Time(min)	Removal(%)
1	8	30	11	60	15	78.76
2	8	5	11	25	15	15.31
3	5	30	7	42.5	10	46.1
4	5	17.5	7	25	10	49.61
5	8	30	11	25	5	20.04
6	5	17.5	7	42.5	10	62.76
7	2	5	3	25	15	11.22
8	5	17.5	3	42.5	10	83.56
9	8	5	3	25	5	29.07
10	5	17.5	11	42.5	10	50.34
11	8	30	3	25	15	65.23
12	2	5	11	25	5	5.15
13	5	17.5	7	42.5	10	58.33
14	2	30	11	25	15	11.78
15	2	30	11	60	5	37.13
16	8	5	11	60	5	42.53
17	2	5	11	60	15	30.01
18	5	17.5	7	42.5	10	61.36
19	5	17.5	7	42.5	5	45.83
20	5	17.5	7	42.5	10	66.51
21	5	17.5	7	42.5	15	81.3
22	2	30	3	25	5	21.23
23	2	5	3	60	5	41.12
24	8	30	3	60	5	92.79
25	5	17.5	7	42.5	10	59.8
26	2	17.5	7	42.5	10	36.88
27	8	17.5	7	42.5	10	76.79
28	5	17.5	7	42.5	10	62.16
29	5	17.5	7	60	10	85.03
30	2	30	3	60	15	45.19
31	5	5	7	42.5	10	35.54
32	8	5	3	60	15	65.74

Table 3 pH monitor of AMR degradation by PS/ZVI

pH i	pH f
3	2.7
5	2.85
7	2.9
9	3.4
11	5.5

parameters values for AMR target removal were PDS concentration = 7.33 mM, ZVI dosage = 17.79 mM, initial pH 4.62, temperature = 59.49 °C, reaction time = 9.88 min. However, this study still have some limitation. Future study should pay more attention on the change in ferrous ion concentration because the ferrous ion is the substance to directly activate the PDS. The degradation efficiency and natural organic matter for the practical wastewater treatment should be studied.

Table 4 Analysis of variance (ANOVA) results of quadratic model for AMR removal

Source	Sum of squares	*df*	Mean square	*F*-value	*p*-value
Model	15,820.68	20	791.03	23.53	< 0.0001
A-PDS	3487.52	1	3487.52	103.75	< 0.0001
B-ZVI	1066.60	1	1066.60	31.73	0.0002
C-pH	1285.25	1	1285.25	38.24	< 0.0001
D-Tem	4283.06	1	4283.06	127.42	< 0.0001
E-time	105.85	1	105.85	3.15	0.1036
AB	258.73	1	258.73	7.70	0.0181
AC	206.64	1	206.64	6.15	0.0306
AD	110.78	1	110.78	3.30	0.0968
AE	162.82	1	162.82	4.84	0.0500
BC	44.16	1	44.16	1.31	0.2761
BD	27.41	1	27.41	0.82	0.3859
BE	28.52	1	28.52	0.85	0.3768
CD	2.30	1	2.30	0.068	0.7987
CE	99.20	1	99.20	2.95	0.1138
DE	71.91	1	71.91	2.14	0.1715
A^2	116.02	1	116.02	3.45	0.0901
B^2	1288.35	1	1288.35	38.33	< 0.0001
C^2	25.97	1	25.97	0.77	0.3982
D^2	32.22	1	32.22	0.96	0.3486
E^2	3.18	1	3.18	0.095	0.7642
Residual	369.75	11	33.61		
Lack of Fit	294.64	6	49.11	3.27	0.1073
Pure Error	75.11	5	15.02		
Cor Total	16,190.43	31			

Table 5 Coefficients in terms of coded factors

Factor	Coefficient Estimate	Standard Error	95% CI Low	95% CI High
Intercept	63.11	1.59	59.70	66.71
A-PS	13.92	1.31	10.81	16.59
B-Fe	7.70	1.31	5.03	10.81
C-pH	−8.45	1.31	−12.00	−6.23
D-Tem	15.43	1.31	13.20	18.98
E-time	2.43	1.31	−1.13	4.65
AB	4.02	1.39	1.71	7.83
AC	3.59	1.39	−6.91	−0.7805
AD	2.63	1.39	−0.1820	5.94
AE	3.19	1.39	−0.1232	6.00
BC	−1.66	1.39	−4.47	1.65
BD	1.31	1.39	−2.00	4.12
BE	1.33	1.39	−1.48	4.65
CD	0.38	1.39	−1.93	4.19
CE	2.49	1.39	−1.32	4.80
DE	−2.12	1.39	−4.43	1.69
A^2	−6.87	3.55	−14.84	0.7772
B^2	−22.88	3.55	−30.86	−15.24
C^2	3.25	3.55	−4.73	10.89
D^2	3.62	3.55	−4.36	11.26
E^2	−1.14	3.55	−9.11	6.51

Acknowledgements The authors are very thankful and acknowledge to Engineering Research Center for Water Environment Ecology of Shanghai Ocean University. We also thank the reviewers and editors for their valuable advice to improve this manuscript.

Author contributions CY: Conceptualization, Methodology, Software, Formal analysis, Investigation, Validation, Writing-Original Draft, Writing-review & editing. XL: Conceptualization, Methodology, Writing-Review & Editing. JL: Investigation. YZ: Writing-Review & Editing.

Funding This work was financially supported by China Postdoctoral Science Foundation (2018M641983) and the Ocean-river-lake Biological Chain Construction and Resource Utilization Engineering Technology Research Center (Grant No. 20DZ2250700).

Data availability The data that support the findings of this study are available from the corresponding author upon reasonable request.

Declarations

Conflict of interest The authors declare that they have no competing interests.

Ethical approval This article does not contain any studies with animals performed by any of the authors.

References

1. Sudrajat H, Babel S (2016) Rapid pH otocatalytic degradation of the recalcitrant dye amaranth by highly active N-WO_3. Environ Chem Lett 14(2):243–249
2. Mittal A, Kurup L, Gupta VK (2005) Use of waste materials—bottom ash and de-oiled soya, as potential adsorbents for the removal of amaranth from aqueous solutions. J Hazard Mater 117(2–3):171–178
3. Wang B, Chen PY, Zhao RX, Zhang L, Chen Y, Yu LP (2020) Carbon-dot modified polyacrylonitrile fibers: recyclable materials capable of selectively and reversibly adsorbing small-sized anionic dyes. Chem Eng J 391:123484
4. Chung K-T, Fulk GE, Egan M (1978) Reduction of azo dyes by intestinal anaerobes. Appl Environ Microbiol 35(3):558–562
5. Lee J, Von Gunten U, Kim J-H (2020) Persulfate-based advanced oxidation: critical assessment of opportunities and roadblocks. Environ Sci Technol 54(6):3064–3081
6. Ma J, Zhang Q, Chen F, Zhu Q, Wang Y, Liu G (2020) Remediation of PBDEs-metal co-contaminated soil by the combination of metal stabilization, persulfate oxidation and bioremediation. ChemospH ere 252:126538

7. Chen F, Huang G-X, Yao F-B, Yang Q, Zheng Y-M, Zhao Q-B, Yu H-Q (2020) Catalytic degradation of ciprofloxacin by a visible-light-assisted peroxymonosulfate activation system: performance and mechanism. Water Res 173:115559
8. Ghauch A, Tuqan AM, Kibbi N (2012) Ibuprofen removal by heated persulfate in aqueous solution: a kinetics study. Chem Eng J 197:483–492
9. Sun C, Chen T, Huang Q, Zhan M, Li X, Yan J (2020) Activation of persulfate by CO_2-activated biochar for improved pH enolic pollutant degradation: performance and mechanism. Chem Eng J 380:122519
10. Watts RJ, Ahmad M, Hohner AK, Teel AL (2018) Persulfate activation by glucose for in situ chemical oxidation. Water Res 133:247–254
11. Zhang YQ, Du XZ, Huang WL (2011) Temperature effect on the kinetics of persulfate oxidation of p-chloroaniline. Chin Chem Lett 22(3):358–361
12. Yang L, Xue J, He L, Wu L, Ma Y, Chen H, Li H, Peng P, Zhang Z (2019) Review on ultrasound assisted persulfate degradation of organic contaminants in wastewater: Influences, mechanisms and prospective. Chem Eng J 378:122146
13. Liu D, Li M, Li X, Ren F, Sun P, Zhou L (2020) Core-shell Zn/Co MOFs derived Co_3O_4/CNTs as an efficient magnetic heterogeneous catalyst for persulfate activation and oxytetracycline degradation. Chem Eng J 387:124008
14. Lin K-YA, Chang H-A, Hsu C-J (2015) Iron-based metal organic framework, MIL-88A, as a heterogeneous persulfate catalyst for decolorization of Rhodamine B in water. RSC Adv 5(41):32520–32530
15. Naim S, Ghauch A (2016) Ranitidine abatement in chemically activated persulfate systems: assessment of industrial iron waste for sustainable applications. Chem Eng J 288:276–288
16. Wang S, Wu J, Lu X, Xu W, Gong Q, Ding J, Dan B, Xie PJCEJ (2019) Removal of acetaminopH en in the Fe^{2+}/persulfate system: kinetic model and degradation pathways. Chem Eng J 358:1091–1100
17. Wei X, Gao N, Li C, Deng Y, Zhou S, Li L (2016) Zero-valent iron (ZVI) activation of persulfate (PS) for oxidation of bentazon in water. Chem Eng J 285:660–670
18. Hussain I, Zhang Y, Huang S (2014) Degradation of aniline with zero-valent iron as an activator of persulfate in aqueous solution. RSC Adv 4(7):3502–3511
19. Le C, Wu J-H, Li P, Wang X, Zhu N-W, Wu P-X, Yang B (2011) Decolorization of anthraquinone dye reactive blue 19 by the combination of persulfate and zero-valent iron. Water Sci Technol 64(3):754–759
20. Eslami A, Asadi A, Meserghani M, Bahrami H (2016) Optimization of sonochemical degradation of amoxicillin by sulfate radicals in aqueous solution using response surface methodology (RSM). J Mol Liq 222:739–744
21. Ahmadi M, Vahabzadeh F, Bonakdarpour B, Mofarrah E, Mehranian M (2005) Application of the central composite design and response surface methodology to the advanced treatment of olive oil processing wastewater using Fenton's peroxidation. J Hazard Mater 123(1–3):187–195
22. Rosa PA, Azevedo AM, Aires-Barros MR (2007) Application of central composite design to the optimisation of aqueous two-pH ase extraction of human antibodies. J Chromatogr A 1141(1):50–60
23. Asghar A, AbdulRaman AA, Daud WMAW (2014) A comparison of central composite design and Taguchi method for optimizing Fenton process. Scientific World J 2014:1–8
24. Geyikçi F, Kılıç E, Çoruh S, Elevli S (2012) Modelling of lead adsorption from industrial sludge leachate on red mud by using RSM and ANN. Chem Eng J 183:53–59
25. Mandal S, Mahapatra S, Patel R (2015) Enhanced removal of Cr (VI) by cerium oxide polyaniline composite: optimization and modeling approach using response surface methodology and artificial neural networks. J Environ Chem Eng 3(2):870–885
26. Liang C, Huang C-F, Mohanty N, Kurakalva RM (2008) A rapid spectropH otometric determination of persulfate anion in ISCO. ChemospH ere 73(9):1540–1543
27. Weng C-H, Tsai K-LJUS (2016) Ultrasound and heat enhanced persulfate oxidation activated with Fe^0 aggregate for the decolorization of CI Direct Red 23. Ultrason Sonochem 29:11–18
28. Wang S, Zhou NJUS (2016) Removal of carbamazepine from aqueous solution using sono-activated persulfate process. Ultrason Sonochem 29:156–162
29. Ferkous H, Merouani S, Hamdaoui O, Pétrier CJUS (2017) Persulfate-enhanced sonochemical degradation of napH thol blue black in water: evidence of sulfate radical formation. Ultrason Sonochem 34:580–587
30. Brlenic V, Kusic H, Juretic D (2016) Comparative study on pH otooxidative treatment of diclofenac: response surface and mechanistic modeling. Ultrason Sonochem 10:78–88
31. Pan X, Yan L, Qu R, Wang Z (2018) Degradation of the UV-filter benzopH enone-3 in aqueous solution using persulfate activated by heat, metal ions and light. ChemospH ere 196:95–104
32. Liang C, Wang ZS, Bruell CJ (2007) Influence of pH on persulfate oxidation of TCE at ambient temperatures. ChemospH ere 66(1):106–113
33. Liang C, Su HW (2009) Identification of sulfate and hydroxyl radicals in thermally activated persulfate. Ind Eng Chem Res 48(11):5558–5562
34. Cui H, Tian Y, Zhang J, Ma S, Li L, Zuo W, Zhang L, Wang TJCEJ (2021) Enhanced oxidation of sulfadiazine by two-stage ultrasound assisted zero-valent iron catalyzed persulfate process: factors and pathways. Chem Eng J 417:128152
35. House DA (1962) Kinetics and mechanism of oxidations by peroxydisulfate. Chem Rev 62(3):185–203
36. Hayon E, Dogliotti LJT (1967) Flash pH otolysis of persulfate ions in aqueous solutions. Study of the sulfate and ozonide radical anions. J PH ys Chem 71:2511–2516
37. Waldemer RH, Tratnyek PG, Johnson RL, Nurmi JTJ (2007) Oxidation of chlorinated ethenes by heat-activated persulfate: kinetics and products. Environ Sci Technol 41(3):1010–1015
38. Liu S, Feng H, Tang L, Dong H, Wang J, Yu J, Feng C, Liu Y, Luo T, Ni T (2020) Removal of Sb(III) by sulfidated nanoscale zerovalent iron: the mechanism and impact of environmental conditions. Sci Total Environ 736:139629
39. Bennedsen LR, Muff J, Søgaard EGJC (2012) Influence of chloride and carbonates on the reactivity of activated persulfate. ChemospH ere 86(11):1092–1097
40. Yang W, Wu T (2019) Investigation of matrix effects in laboratory studies of catalytic ozonation processes. Ind Eng Chem Res 58(8):3468–3477
41. Chen S, Cai M, Liu Y, Zhang L, Feng L (2019) Effects of water matrices on the degradation of naproxen by reactive radicals in the UV/peracetic acid process. Water Res 150:153–161
42. Zou L, Wang Y, Huang C, Li B, Lyu J, Wang S, Lu H, Li J (2021) Meta-cresol degradation by persulfate through UV/O_3 synergistic activation: contribution of free radicals and degradation pathway. Sci Total Environ 754:142219
43. Khan JA, He X, Shah NS, Sayed M, Khan HM, Dionysiou DD (2017) Degradation kinetics and mechanism of desethyl-atrazine and desisopropyl-atrazine in water with OH and SO_4—based-AOPs. Chem Eng J 325:485–494
44. Islahuddin NKS, Halmi MIE, Manogaran M, Shukor MY (2017) Isolation and culture medium optimisation using one-factor-at-time and response surface methodology on the biodegradation of the azo-dye amaranth. Bioremediation Sci Technol Res 5(2):25–31

45. Gomi N, Yoshida S, Matsumoto K, Okudomi M, Konno H, Hisabori T, Sugano Y (2011) Degradation of the synthetic dye amaranth by the fungus Bjerkandera adusta Dec 1: inference of the degradation pathway from an analysis of decolorized products. Biodegradation 22(6):1239–1245
46. Roşu M-C, Socaci C, Floare-Avram V, Borodi G, Pogăcean F, Coroş M, Măgeruşan L, Pruneanu S (2016) PH otocatalytic performance of grapH ene/TiO_2-Ag composites on amaranth dye degradation. Mater Chem PH ys 179:232–241
47. Lin K-YA, Lin T-Y, Chen Y-C, Lin Y-F (2017) Ferrocene as an efficient and recyclable heterogeneous catalyst for catalytic ozonation in water. Catal Commun 95:40–45